Dual-Broadband Highly Efficient Reflective Multi-Polarisation Converter Based on Multi-Order Plasmon Resonant Metasurface

Qi Zheng[1,2*], Chenjiang Guo[1], Guy A. E. Vandenbosch[2], Pengliang Yuan[1], Jun Ding[1]

[1] School of Electronics and Information, Northwestern Polytechnical University, Xi'an China,
[2] ESAT-TELEMIC Research Division, Department of Electrical Engineering, KU Leuven, Leuven, Belgium.
[*] zhq930908@mail.nwpu.edu.cn

Abstract: In this paper, a dual-broadband reflective polarisation converter with high efficiency for both linear-to-linear and linear-to-circular polarisations based on a metasurface is proposed. Owing to the characteristics of strong anisotropy and multi-order plasmon resonances, the proposed polarisation converter can rotate an *y*/*x* polarized electromagnetic (EM) wave to its cross-polarized (*x*/*y*) direction in the lower frequency band of 7.74-14.44 GHz (a fractional bandwidth of 60.4%) with over 0.9 polarisation conversion ratio (PCR). Besides, the proposed structure can also convert a linearly polarized (LP) incident wave to a circularly polarized (CP) one after reflection in the higher frequency band of 14.95-17.35 GHz (a fractional bandwidth of 14.9%). The performance in the two bands can be controlled separately by altering the proper parameters of the structure. Numerical analysis is used to predict the polarisation states of the proposed polarisation converter. Moreover, the physical mechanism of multiple resonances is discussed based on surface current distributions. A prototype of the polarisation converter is fabricated and measured. A reasonable agreement between the experiments and simulations is obtained. The design has a simple and scalable geometry, and is a good candidate for polarisation control devices in microwave, terahertz and optical frequency regions.

1. Introduction

Metasurfaces, two-dimensional metamaterials with a unit cell size and thickness much smaller than a wavelength, have attracted a lot of interest in the fields of polarisation manipulation [1-3], radar cross section reduction [4], antenna design [5], etc. Recently, many metasurface-based reflective polarisation converters have been proposed to manipulate polarisation states of an electromagnetic (EM) wave, taking into account the advantages of low-profile, light weight and flexible design of a metasurface [6-10]. For example, transmission-type circular polarisers have been used to obtain two different polarisations in two bands to create two different channels for up- and down-link satellite communications [11-13]. A dual-band reflection-type circular polariser was proposed to design Cassegrain antennas [14].

Many types of multi-order plasmon resonators have been investigated that rotate a linearly polarized (LP) incident wave into its orthogonal counterpart after reflection, i.e. the polarisation rotator [15-25]. Further, various metasurfaces with anisotropic impedances have been used to convert a LP incident wave into a circularly polarized (CP) one [26-29]. For example, a double split resonant square ring was used in [27] to achieve linear-to-circular polarisation conversion in the Terahertz region within an 80% relative bandwidth. A multi-layered structure was proposed in [28] to expand the operating bandwidth in the frequency range of 4.7-21.7 GHz at normal incidence. However, there is very little research focusing on the multi-polarisation converter, a device very useful in many applications.

In the literature, Jiang *et al.* [30] have shown that the polarisation states of light can be freely tuned by adjusting the structural parameters. In [31] a broadband metamaterial-based reflector has been introduced to convert LP incident waves to cross-polarized reflected waves or CP waves by adjusting dimensional parameters. In [32] a double-L-shaped structure has been proposed to obtain a multi-band multi-polarisation converter. However, the cross polarisation conversion bands are narrow. A multi-polarisation converter has been proposed in [33], while it is a challenge to design this structure in other frequency ranges owing to the coupling effect between the meander-lines and the cut-wire.

In this paper, a broadband and highly efficient reflective polarisation converter based on metasurface working in microwave region is proposed. An LP incident EM wave can be converted to an LP reflected wave (LP-to-LP) in the lower band and a CP reflected wave (LP-to-CP) in the higher band with high efficiency. Physical insight is given, and the performance is investigated by numerical calculations. A parametric study is performed, which provides a guideline for the design in other frequency bands. The structure is finally verified in experiments. The structure could also be rescaled to work in another frequency region. In the THz frequency range, fabrication techniques become a real issue [34].

2. Design and simulations of the metasurface

Fig. 1 presents the scheme of the proposed dual-broadband reflective polarisation converter. This device is comprised of a metasurface-based anisotropic medium, which converts an LP incident wave ($\vec{E}_y^i$) into its cross-polarized direction ($\vec{E}_x^r$) in the lower band and a CP reflected wave ($\vec{E}^r$) in the higher band with high efficiency. The proposed multi-function reflective polarisation converter is a single panel composed of identical unit cells.

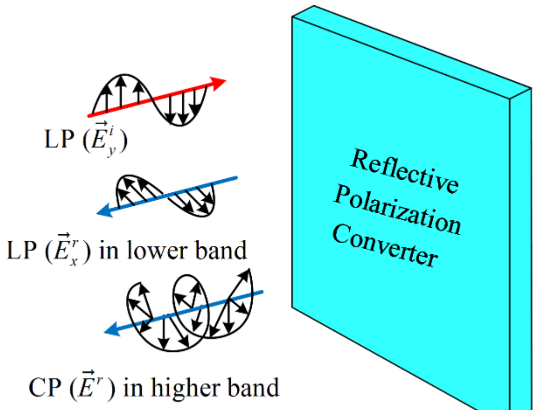

Fig. 1 *Scheme of the proposed LP-to-LP and LP-to-CP reflective metasurface-based polarisation converter*

Fig. 2 gives the schematic top/side view of the unit cell of the proposed metasurface. The unit cell is composed of an H-shaped patch and a metallic ground plate separated by a dielectric substrate layer. The H-shaped patch and metal ground plane are designed by using copper with a conductivity of 5.8×10^7 S/m and a thickness of 0.035 mm. The substrate used is FR-4 with a relative permittivity 4.4 and a loss tangent of 0.02. The unit cell of the polarisation converter is simulated and calculated by using the commercial software Ansoft HFSS vs. 13.0, in which we set a Floquet port in the +*z* direction with wave vector along the –*z* direction and Master/Slave boundaries in +*x*/-*x* and +*y*/-*y* directions, respectively. The final parameters of the geometry are $p=9$ mm, $h=3$ mm, $l_0=3.75$ mm, $w_0=0.4$ mm, $l_1=5$ mm, $l_2=6$ mm, $w_1=0.25$ mm.

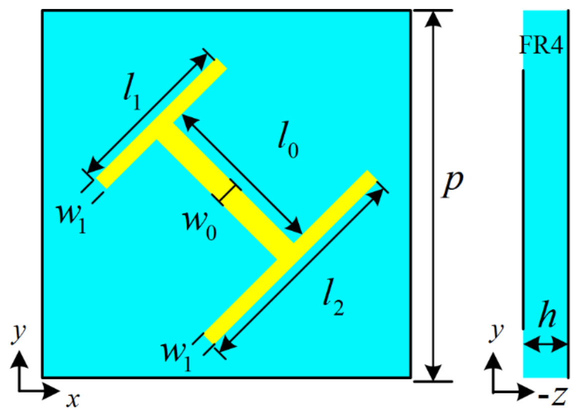

Fig. 2 *Schematic view of the unit cell*

Taking a linearly polarized (LP) electromagnetic (EM) wave along *y*-axis ($\vec{E}_y^i=\vec{y}\left|\vec{E}_y^i\right|$) as an example, the reflected wave consists of both *y*- and *x*-polarized components ($\vec{E}_{\text{total}}^r=\vec{E}_x^r+\vec{E}_y^r$ $=\vec{x}r_{xy}\left|\vec{E}_y^r\right|e^{-j\left(kz+\varphi_{xy}\right)}+\vec{y}r_{yy}\left|\vec{E}_y^r\right|e^{-j\left(kz+\varphi_{yy}\right)}$).Where $r_{xy}=\left|\vec{E}_x^r\right|/\left|\vec{E}_y^i\right|$ and $r_{yy}=\left|\vec{E}_y^r\right|/\left|\vec{E}_y^i\right|$ represent the reflection ratio of *y*-to-*x* (cross-polarisation) and *y*-to-*y* polarisation conversion (co-polarisation), and φ_{xy} and φ_{yy} are the corresponding phases.

The Polarisation Conversion Ratio is defined as $\text{PCR}=r_{xy}^2/\left(r_{xy}^2+r_{yy}^2\right)=1-r_{yy}^2/\left(r_{xy}^2+r_{yy}^2\right)$ [15]. It is employed to evaluate the efficiency of cross polarisation conversion. The axial ratio (AR, $\text{AR}=\left(\left(r_{xy}^2+r_{yy}^2+\sqrt{a}\right)/\left(r_{xy}^2+r_{yy}^2-\sqrt{a}\right)\right)^2$, where $a=r_{xy}^4+r_{yy}^4$ $+2r_{xy}^2r_{yy}^2\cos(2\Delta\varphi_{xy})$, $\Delta\varphi_{xy}=\varphi_{xy}-\varphi_{yy}$ [32]) of the reflected wave is given to characterize the bandwidth of the linear-to-circular polarisation.

Fig. 3(a) presents the simulated reflection coefficients of co-polarisation (r_{yy}) and cross-polarisation (r_{xy}). It is shown that the r_{yy} is less than -10 dB in the band of 7.7-14.5 GHz and r_{xy} is over -1.5 dB in the band of 8.0-14.0 GHz. Four resonances occur at 8.04, 10.82, 12.71 and 14.23 GHz. Fig. 3(b) gives the phase difference between *x*- and *y*-components of the reflected EM wave. A 90° relative phase difference can be obtained in the high band of 14.82-17.68 GHz.

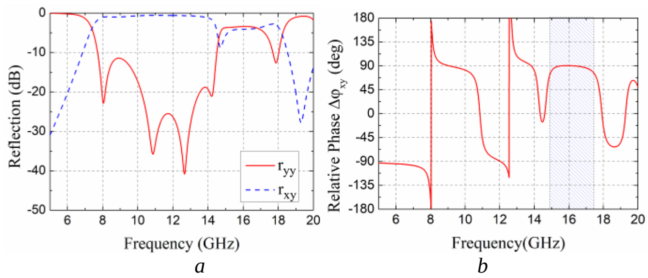

Fig. 3 *Simulated results of reflection coefficients and phase difference*

(a) Co- and cross-polarisation coefficients, ***(b)*** Reflective phase difference between *x*- and *y*-components

As shown in Fig. 4, the structure achieves over 0.9 PCR in the lower band (LP-to-LP) of 7.74-14.44 GHz, where nearly 1.0 PCR can be achieved at the four resonances. This means that most energy of the *y*-polarized wave is rotated to the *x*-polarized one after being reflected by the metasurface. It can also be seen that the r_{yy} and r_{xy} are roughly equal at 16.0 ± 1.0 GHz from Fig. 3(a), which shows the nearly equal reflection magnitudes along *x*- and *y*-direction of the reflected wave. The axial ratio (AR) values are shown in Fig. 4. The AR is less than 3-dB from 14.95 to 17.35 GHz, which indicates a circular polarisation state (LP-to-CP). The 90° phase difference in Fig. 3(b) indicates a right-hand circular polarisation.

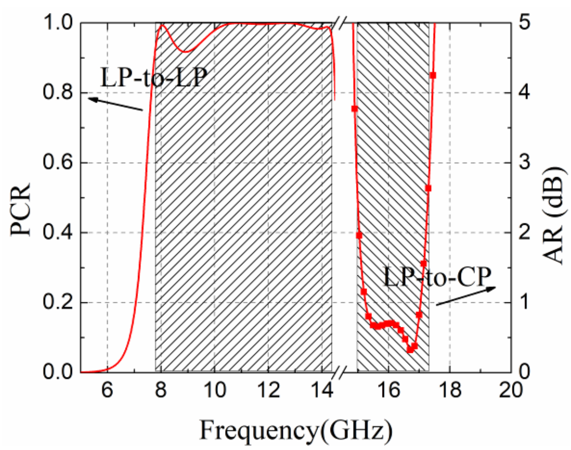

Fig. 4 *PCR and AR.*

Fig. 5 gives the PCR and AR of the proposed polarisation converter under oblique incidence for TE/TM modes. It is noted that

$\mathrm{PCR} = r_{xy}^2 / (r_{xy}^2 + r_{yy}^2)$ for the TE mode and $\mathrm{PCR} = r_{yx}^2 / (r_{yx}^2 + r_{xx}^2)$ for the TM mode in the cross-polarisation low frequency conversion band. It can be concluded from Fig. 4 that when the incident angle (θ) changes from 0° to 30°, the PCR stays stable from 11 to 14 GHz for both the TE and TM modes, while in the lowest band it changes slightly. The PCR is over 0.88 at $\theta = 20^\circ$ and the cross–polarisation bandwidth does not change, except for a slight variation in the high frequency region. In the high band of linear-to-circular polarisation conversion, the AR characteristics shift to lower frequencies and show a relative 3-dB AR bandwidth at $\theta = 20^\circ$ of about 10%. This value deteriorates greatly at $\theta = 30^\circ$. Summarizing, the proposed metasurface keeps a good polarisation conversion characteristic in the range up to maximum 20° from oblique incidence.

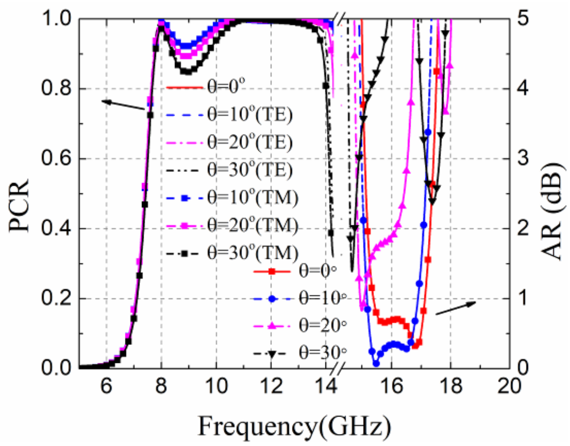

Fig. 5 *PCR and AR at different incident angles*

3. Theoretical Analysis and Physical Mechanism

In this part, principles of linear-to-linear and linear-to-circular conversion are analyzed based on numerical calculation and surface current distributions, respectively.

The proposed design starts from an "H" shaped structure anisotropic metamaterial, which has been studied extensively in literature [15], [20]. It has been proved in [15] that all possible polarization states can be manipulated by the structure via the adjusting of parameters. In [20] a "H" shaped reflective polarization rotator was proposed for wideband and wide-angle LP-to-LP polarization conversion. Different from these references, but based on the same H shape in our work the structure is developed for dual-band dual-polarization conversions. Basically, the proposed H-shaped structure is a connection of two cut-wires parallel to the diagonal direction and one cut-wire perpendicular to the two parallel cut-wires. The polarization state of the reflected wave can be manipulated through varying the length and width of the three cut-wires, corresponding to adjusting the reflection coefficients and phases along two orthogonal directions.

The performance of the polarisation conversion can be attributed to the anisotropic property with "symmetric" and "anti-symmetric" modes [1]. Thus the *y*-polarized incident EM wave ($\vec{E}_y^i$) can be decomposed into two perpendicular equal components along the *u*-axis ($\vec{E}_u^i$) and the *v*-axis ($\vec{E}_v^i$), which are $\pm 45^\circ$ rotated with respect to the +*y*-axis, as shown in Fig. 6(a). The LP incident EM field can be expressed as

$$\vec{E}_y^i = \vec{y} E_0 e^{jkz} = \vec{E}_u^i + \vec{E}_v^i = \vec{u}\left|\vec{E}_u^i\right| e^{jkz} + \vec{v}\left|\vec{E}_v^i\right| e^{jkz} \quad (1)$$

where $\left|\vec{E}_u^i\right| = \left|\vec{E}_v^i\right| = \left(\sqrt{2}/2\right) E_0$.

The reflection coefficients along the *u*- and *v*-axis can be written as r_u and r_v, so the reflected EM wave can be expressed as

$$\vec{E}^r = \vec{E}_u^r + \vec{E}_v^r = \vec{u} r_u \left|\vec{E}_u^i\right| e^{j(kz+\varphi_u)} + \vec{v} r_v \left|\vec{E}_v^i\right| e^{j(kz+\varphi_v)} \quad (2)$$

When the reflection coefficients $r_u = r_v = r$ and phase difference $|\varphi_u - \varphi_v| = \pi$, we get

$$\vec{E}^r = \left(\sqrt{2}/2\right) r E_0 e^{j(kz+\varphi_v)} \left(\vec{u} e^{j\pi} + \vec{v}\right) \quad (3)$$

As a result, the reflected wave has a linear polarization, which means that LP-to-LP polarization conversion is obtained.

When the reflection coefficients $r_u = r_v = r$ and phase difference $|\varphi_u - \varphi_v| = \pi/2$, we get

$$\vec{E}^r = \left(\sqrt{2}/2\right) r E_0 e^{j(kz+\varphi_v)} \left(\vec{u} e^{j\pi/2} + \vec{v}\right) \quad (4)$$

As a result, the reflected wave has a circular polarization, which means that LP-to-CP polarization conversion is obtained.

The simulated reflection coefficients and reflection phases of the *u*- and *v*-components are depicted in Fig. 6(b). It can be concluded that the reflection coefficients are roughly equal ($r_u \approx r_v$) and the reflection phase differences in the two bands are around $|\varphi_u - \varphi_v| = 180^\circ$ and $|\varphi_u - \varphi_v| = 90^\circ$, respectively. This indicates that linear-to-linear and linear-to-circular polarisation conversion can be obtained in the two bands, respectively. It should be noted that the two bands predicted by the theoretical analysis show slight differences compared with the two bands predicted by the commercial software. These discrepancies are reasonable because the theoretical calculations are analyzed based on the consideration of perfect LP and CP reflected EM waves, but the simulated results are evaluated taking into account the 0.9 PCR for linear-to-linear polarization conversion in the lower frequency band and 3-dB AR for the linear-to-circular polarization conversion in the higher frequency band. However, the theoretical model can still serve to give a first simple working mechanism of the polarization conversion process.

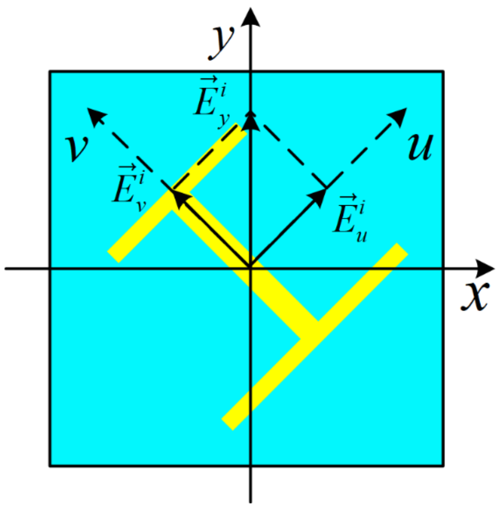

a

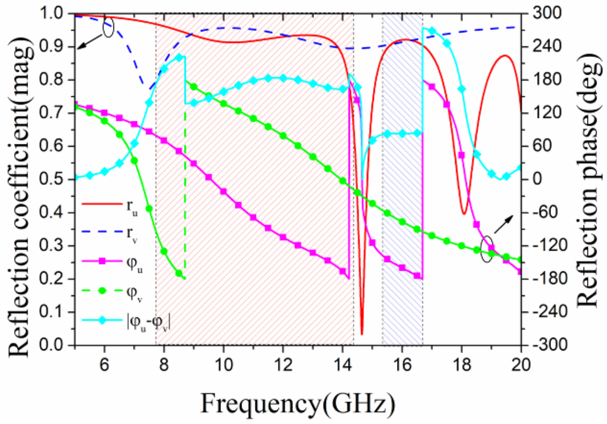

b

Fig. 6 *New coordinate system and simulated results*

(a) *u*- and *v*-axis coordinate system. ***(b)*** Reflection coefficients and phases for *u*- and *v*-polarisation.

The anti-symmetric and symmetric modes generated by the front and bottom metal parts result in the magnetic and electric dipole responses [1], [6], [28], respectively. Fig 7 shows the induced surface current in the top and bottom metals at the four resonance frequencies (8.04, 10.82, 12.71 and 14.23 GHz) of the linear-to-linear polarisation conversion. It can be seen from Fig. 7(a) that at 8.04 GHz the total induced current in the front metal flows in the diagonal direction from up left to down right. The current in the bottom layer is in the opposite direction at this frequency. This corresponds to a magnetic dipole resonance. The *y* component of the induced magnetic field parallel to the electric field of the incident wave leads to the conversion of a *y*-polarized incident field to an *x*-polarized reflected field. As shown in Fig. 7(b), the induced currents in the top and bottom metals are opposite, which corresponds to magnetic resonance at 10.82 GHz. According to Fig. 7(c), the surface currents in the front and bottom metals at 12.71 GHz flow in nearly the same direction, which corresponds to an electric dipole resonance. The *x* component of the induced electric field is rotated into a cross-polarized component. Similar results can be obtained from Fig. 7(d), both the currents in the two metal parts at 14.23 GHz flow from down right to up left.

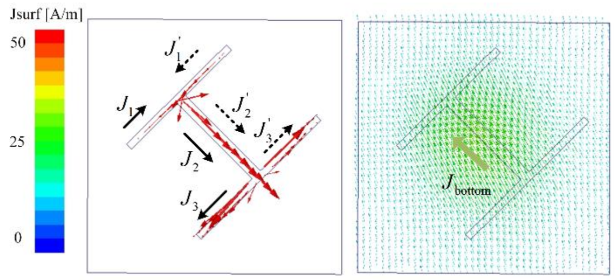

a

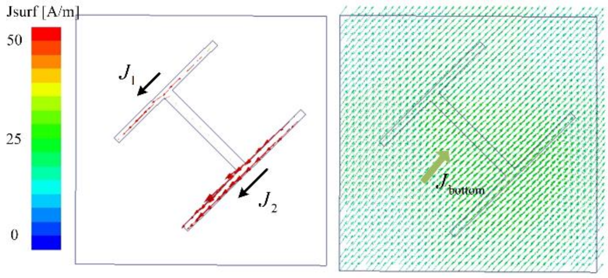

b

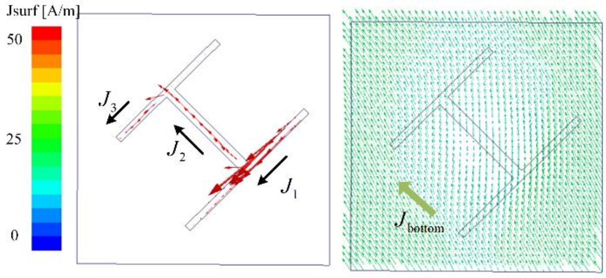

c

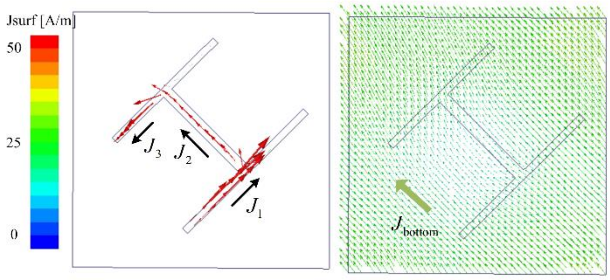

d

Fig. 7 *Induced surface current on top and bottom metallic parts of the unit cell at the four resonances of the linear-to-linear polarisation conversion.*

(a) 8.04 GHz, ***(b)***10.82 GHz, ***(c)***12.71 GHz, ***(d)***14.23 GHz

Fig. 8 gives the surface current distributions at the center frequency (16.10 GHz) for the linear-to-circular polarisation conversion. These currents flow in two directional paths: one is from down left to up right (J_{total}) and another one (J'_{total}) is from down right to up left, which means that they flow in nearly orthogonal directions. Thus, the lengths and widths of the two parallel cut-wires and one perpendicular cut-wire can be adjusted properly to obtain linear-to-circular polarisation conversion.

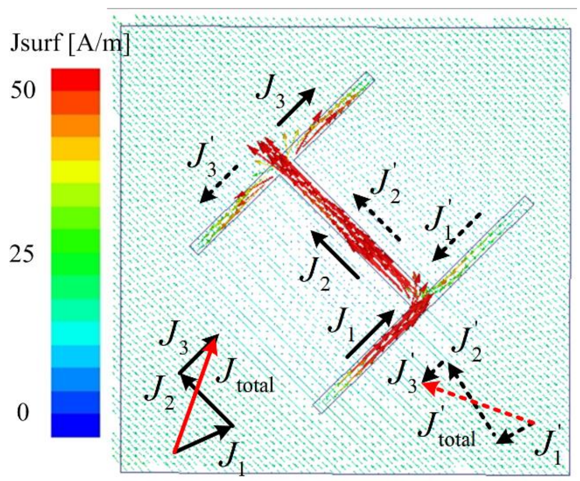

Fig. 8 *Induced surface current on top and bottom metallic parts at 16.10 GHz of linear-to-circular polarisation conversion.*

In order to understand the effects of each part of the structure, several parameters are investigated in detail. The influence of the substrate thickness h on the polarisation conversion performance is shown in Fig. 9(a). The other parameters are kept constant. In the low frequency linear-to-linear conversion band, the PCR performs better. However, in the higher frequency region it deteriorates violently when h increases. For the linear-to-circular conversion band, the two minimum AR points shift to a higher frequency with the increasing of the substrate thickness. Fig. 9(b) gives the PCR and AR versus the arm length l_1. When l_1 increases, the PCR of the linear-to-linear conversion band remains stable, except for a slight shift to lower frequencies, while the AR of the linear-to-circular conversion band changes greatly. The effect of the center cut-wire length l_0 and arm length l_2 of the H is depicted in Figs. 9(c) and (d). With the increase of l_0 and l_2, there is a shift of the PCR of the linear-to-linear conversion band to lower frequencies, but the AR of the linear-to-circular conversion remains stable. These results mean that both of the two lengths have a key influence on the linear-to-linear polarisation conversion, while they have less impact on the linear-to-circular polarisation conversion.

Figs. 10(a) and (b) display the influence of the widths of the center part w_0 and the two arms w_1. It can be concluded that w_0 affects the AR of the linear-to-linear conversion, but it does almost not affect the PCR of the linear-to-circular conversion. However, w_1 plays an opposite role. It has more impact on the linear-to-circular conversion but less impact on the linear-to-linear conversion.

Summarizing, a dual-band dual-polarisation converter could be obtained by adjusting the substrate thickness and by modifying the top H-shaped structure. The up left arm can be used to tune the LP-to-CP polarization conversion in the high band and the center part and down right arm can be used to tune the LP-to-LP polarization conversion in the low band.

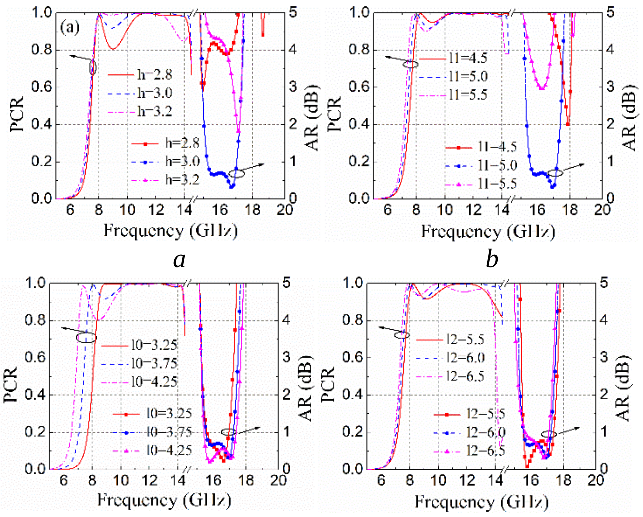

a *b*

c *d*

Fig. 9 *PCR and AR at different parameters* ***(a)*** h, ***(b)*** l_1, ***(c)*** l_0, ***(d)*** l_2,

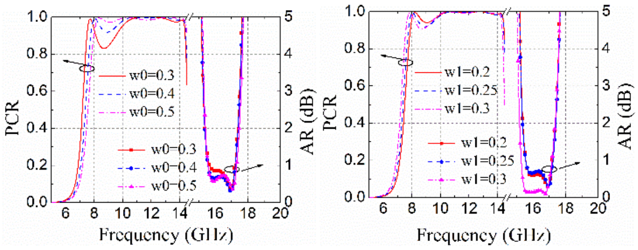

a *b*

Fig. 10 *PCR and AR at different widths* ***(a)*** w_0, ***(b)*** w_1.

4. Measurements

A sample of the broadband multi-function polarisation converter was fabricated, which consists of 30×30 unit cells with an area of 270 mm $\times$ 270 mm $\times$ 3 mm. The prototype is fabricated using printed circuit board (PCB) technology. A schematic illustration of the measurement setup is depicted in Fig. 11(a). In the first step, two identical LP horns are placed along the same direction to ensure the same polarisation. One horn is used as the transmit antenna and the other one is used as the receive antenna to obtain the co-polarized component (r_{yy}) of the reflected EM wave. In the second step, the cross-polarisation component (r_{xy}) of the reflected EM wave is obtained by rotating the receive antenna with 90° and measuring again. The PCR and AR can be calculated using the measured data. It is important to point out that the reflection of an equally sized metallic plate was measured, and served as a reference in order to reduce the influence of the noise of the measurement environment.

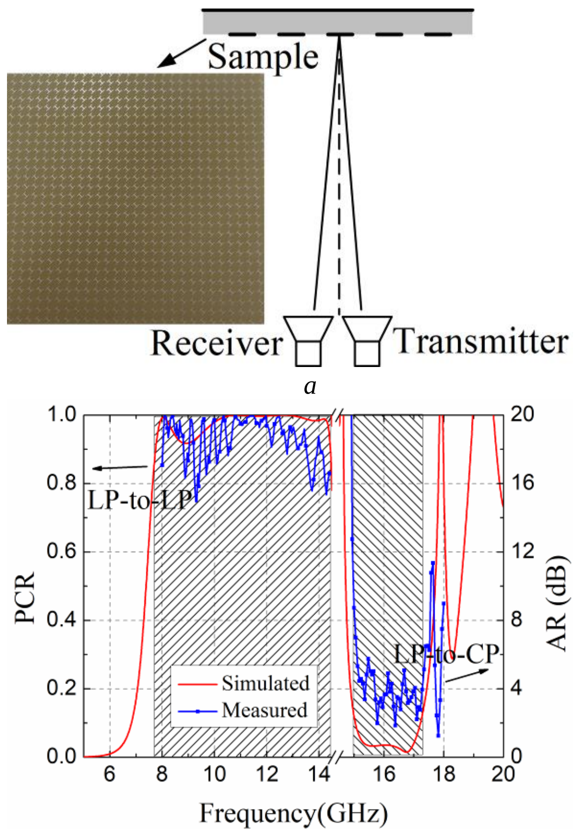

a

b

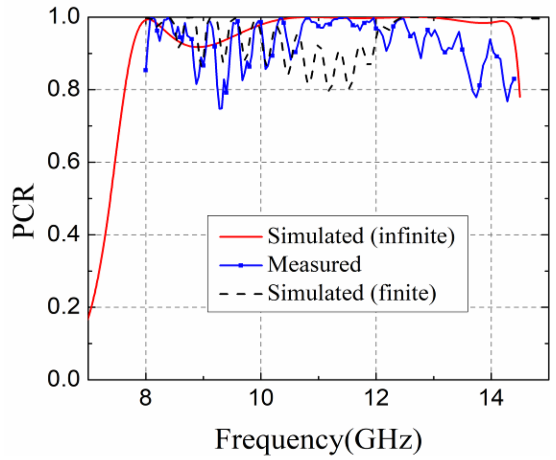

c

Fig. 11 *Measured results and discussion*

(a) Schematic view of the experiment setup. *(b)* Measured and simulated results versus frequency, simulations are for the infinite structure with an impinging normally incident plane wave *(c)* Comparison of simulation of the infinite structure with a full-wave simulation of the finite structure in CST Microwave Studio (the distance between the horn antennas and the sample is 35 cm).

Fig. 11(b) gives the comparison of the measured results and the simulated ones. The unit cell simulations (= infinite structure) were carried out with both HFSS [35] and CST Microwave Studio [36] for mutual verification purposes. The HFSS results for the PCR and AR were retained and are presented here since this software provides an easier post-processing. The simulations of the structure consisting of 30 $\times$ 30 unit cells (= finite structure) were carried out by using CST Microwave Studio, since this software provides a higher speed for this structure. The full-wave simulation includes two horn antennas and the finite structure. Considering the solving time and accuracy, the time domain solver in CST was used due to its high performance when simulating large objects. It can be observed that the measurements and simulations of PCR are in a reasonable agreement, which validates the polarisation conversion performance of the proposed metasurface. The discrepancies between the measured and simulated AR are mainly caused by the difference between the simulated topology (infinite sample, plane waves) and the practical measurement set-up (finite sample, use of horn antennas). The measured phases are sensitive to this. The behavior of the actually realized finite design in the measurement set-up with two horn antennas was also simulated with the full wave solver CST Microwave Studio and is given in Fig. 11(c). This clearly proves that the measured oscillations in Fig. 11(b) are due to the finiteness of the set-up.

An overview of the single-layer metasurface-based polarisation converters in literature is given in Table I. The design proposed in [31] can be used either for broadband linear-to-linear or for linear-to-circular polarisation transformations, depending on the set of design parameters chosen. It cannot realize these transformations at the same time with exactly the same structure. The design proposed in [32] can be used for multiband transformations, just as our design, but the bandwidth of the linear-to-linear polarisation conversion is extremely narrow. Our convertor shows the largest bandwidth, over 60 %, for the linear to linear conversion, and a reasonable performance for the linear to circular conversion simultaneously.

Table I Comparison of polarisation converters in literature

Refs	Center Frequency (GHz)	Performance	FBW (%)
[23]	15.6	LP-to-LP	94.87(PCR>0.9)
[26]	12	LP-to-CP	15
[31] (Part 3.1)	15.75	LP-to-LP	55.5 (PCR>0.8)
[31] (Part 3.2)	13.55	LP-to-CP	30.3
[32]	6.3/10.825/16.925 5.8/8.125/14.05/20.3	LP-to- LP LP-to- CP	Narrow 9.84/36.31/27.76/21.67
this work	11.09 16.15	LP-to-LP LP-to-CP	60.4(PCR>0.9) 14.9

5. Conclusion

A dual-broadband and highly efficient reflective polarisation converter based on anisotropic metasurface for both linear-to-linear and linear-to-circular polarisation conversion is presented. Due to the anisotropic characteristic and multi-order plasmon resonances, the proposed metasurface can convert a *y*/*x*-polarized incident wave to an *x*/*y*-polarized one in the lower frequency band with over 0.9 PCR. Further, the metasurface can also convert an LP incident wave into a circular one in the higher frequency band with less than 3-dB AR. The performance in the two bands can be controlled separately by altering the corresponding parameters. A parametric study is given in detail to serve as a guide for the design. A study of the induced current distributions is presented to explain the operating principle of the polarisation conversions. Both simulated and measured results verify that the proposed metasurface can achieve broadband multi-polarisation conversion at microwave frequencies. Owing to its advantages of simple design and scalable geometry compared to other polarisation converters, the design has potential applications from the microwave to the optical region.

6. Acknowledgments

Authors thank the supports from the China Scholarship Council (No. 201806290108) and the Science Research Project of Gansu Province Higher Educational Institutions (No. 2019A-268).

7. References

[1] Yu, N., Genevet, P., Kats, MA., *et al.*: 'Light propagation with phase discontinuities: generalized laws of reflection and refraction'. *Science*, 2011, p. 1210713.

[2] Chen, H.-T., Taylor, A.J., Yu, N.: 'A review of metasurfaces: physics and applications'. *Rep. Prog. Phys*. 2016, 79, p. 076401.

[3] Guo, W. L., Wang, G. M., Li, H. P., *et al.*: 'Analysis and design of a broadband metasurface-based vortex beam generator'. *IEEE Access*, 2019, 7, pp. 129529-129536.

[4] Zheng, Y-J., Gao, Jun., Zhou, Y-L., *et al.*: 'Metamaterial-based patch antenna with wideband RCS reduction and gain enhancement using improved loading method'. *IET Microw. Antennas Propag.*, 2017, **11**, (9), pp. 1183-1189.

[5] Chen, Q., Zhang, H.: 'Dual-patch polarization conversion metasurface-based wideband circular polarization slot antenna', *IEEE Access*, 2018, 6, pp. 74772-74777.

[6] Grady, N. K., Heyes, J. E., Chowdhury, D. R., *et al.*: 'Terahertz metamaterials for linear polarization conversion and anomalous refraction', *Science*, 2013, p. 1235399.

[7] Gao, X., Yang, W. L., Ma, H. F., *et al.*: 'A reconfigurable broadband polarization converter based on an active metasurface', *IEEE Trans. Antennas Propag.* 2018, **66**, (11), pp. 6086-6095.

[8] Xu, J., Li, R., Wang, S., *et al.*: 'Ultra-broadband linear polarization converter based on anisotropic metasurface', *Opt. Express*, 2018, **26**, (20), pp. 26235-26241.

[9] Huang, X., Yang, H., Zhang, D., *et al.*: 'Ultrathin dual-band metasurface polarization converter', *IEEE Trans. Antennas Propag.* 2019, doi: 10.1109/TAP.2019.2911377.

[10] Lončar, J., Grbic, A., Hrabar, S.: 'A reflective polarization converting metasurface at X-band frequencies', *IEEE Trans. Antennas Propag.*, 2018, **66**, (6), pp. 3213-3218.

[11] Ma, X., Huang, C., Pan, W., *et al.*: 'A dual circularly polarized horn antenna in Ku-band based on chiral meta material', *IEEE Trans. Antennas Propag.*, 2014, **62**, (4), pp. 2307–2311

[12] Barbuto, M., Trotta, F., Bilotti, F., Toscano, A.: 'Design and experimental validation of dual-band circularly polarised horn filtenna', *Electron. Lett.*, 2017, **53**, (10), pp. 641-642.

[13] Jie, R., Jing, H., Li, S., *et al.*: 'Dual-band circular polarizers based on a planar chiral metamaterial structure." *IEEE Antennas Wireless Propag. Lett.* 2019, **18**, (12), pp: 2587-2591.

[14] Fartookzadeh, M., Armaki. S. H. M., 'Dual-band reflection-type circular polarizers based on anisotropic impedance surfaces', *IEEE Trans. Antennas Propag.*, 2015, 64(2), pp. 826-830.

[15] Hao, J., Yuan, Y., Ran, L., *et al*: 'Manipulating electromagnetic wave polarizations by anisotropic metamaterials'. *Phys. Rev. Lett.* 2007, **99**, (6), p. 063908.

[16] Feng, M., Wang, J., Ma, H., *et al.*: 'Broadband polarization rotator based on multi-order plasmon resonances and high impedance surfaces', *J. Appl. Phys.*, 2013, **114**, (7), p. 074508.

[17] Shi, H., Li, J., Zhang, A., *et al.*: 'Broadband cross polarization converter using plasmon hybridizations in a ring/disk cavity," *Opt. Express*, 2014, **22**, (17), pp. 20973-20981.

[18] Jia, Y., Liu, Y., Zhang, W., *et al.*: 'Ultra-wideband and high-efficiency polarization rotator based on metasurface', *Appl. Phys. Lett*. 2016, **109**, (5), p. 051901.

[19] Sun, H., Gu, C., Chen, X., *et al*.: 'Ultra-wideband and broad-angle linear polarization conversion metasurface', *J. Appl. Phys*.,2017, **121**, (17), p. 174902.

[20] Xu, J., Li, R., Qin, J., *et al.*: 'Ultra-broadband wide-angle linear polarization converter based on H-shaped metasurface', *Opt. Express*. 2018, **26**, (16), pp. 20913-20919.

[21] Zhao, J., Cheng, Y. Z., Cheng, Z.: 'Design of a photo-excited switchable broadband reflective linear polarization conversion metasurface for terahertz waves', *IEEE Photonics J.*, 2018, **10**, (1), pp. 1-10.

[22] Li, F., Chen, H., Zhang, L., *et al.*: 'Compact high-efficiency broadband metamaterial polarizing reflector at microwave frequencies', *IEEE Trans. Microw. Theory Tech*, 2018, **67**, (2), pp. 606-614.

[23] Long, F., Yu, S., Kou, N., *et al.*: 'Efficient broadband linear polarization conversion metasurface based on %-shape', *Microw Opt Techn Let.* 2020, **62**, (1), pp. 226-232.

[24] Zheng, Q., Guo, C., G. A. Vandenbosch, *et al.*: 'Ultra-broadband and high-efficiency reflective polarization rotator based on fractal metasurface with multiple plasmon resonances', *Optics Communications*, 2019, 449, pp. 73-78.

[25] Yan, M., Wang, J., Pang, Y., *et al.*: 'An FSS-backed dual-band reflective polarization conversion metasurface', *IEEE Access*, 2019, **7**, pp. 104435-104442.

[26] Ma, H. F., Wang, G. Z., Kong, G. S., *et al.*: 'Broadband circular and linear polarization conversions realized by thin birefringent reflective metasurfaces', *Opt. Mater. Express.*, 2014, **4** (8), pp. 1717-1724.

[27] Jiang, Y., Wang, L., Wang, J., *et al.*: 'Ultra-wideband high-efficiency reflective linear-to-circular polarization converter based on metasurface at terahertz frequencies', *Opt. Express*., 2017, **25,** (22), pp. 27616-27623.

[28] Jia, Y., Liu, Y., Zhang, W., *et al.*: 'Ultra-wideband metasurface with linear-to-circular polarization conversion of an electromagnetic wave', *Opt. Mater. Express*., 2018, **8**, (3), pp. 597-604.

[29] Li, S., Zhang, X.: 'An ultra-wideband linear-to-circular polarization converter in reflection mode at terahertz frequencies', *Microw Opt Techn Let.*, 2019, **61**, pp.2675-2680.

[30] Jiang, S. C., Xiong, X., Hu, Y. S., *et al.*: 'Controlling the polarization state of light with a dispersion-free metastructure', *Phys. Rev. X*, 2014, **4**, (2), p.021026.

[31] Zhang, Z., Cao, X., Gao, J., *et al.*: 'Broadband metamaterial reflectors for polarization manipulation based on cross/ring resonators', *Radioengineering*, 2016, **25**, (2), p.436-441.

[32] Mao, C., Yang, Y., He, X., et al.: 'Broadband reflective multi-polarization converter based on single-layer double-L-shaped metasurface', *Appl. Phys. A.*, 2017, **123**, (12), p. 767.

[33] Zheng, Q., Guo, C., Ding, J.: 'Wideband metasurface-based reflective polarization converter for linear-to-linear and linear-to-circular polarization conversion', *IEEE Antennas Wireless Propag. Lett.*, 2018, **17**, (8), pp. 459-463.

[34] Liu, N., Guo, H., Fu, L., *et al.*: 'Three-dimensional photonic metamaterials at optical frequencies'. *Nature materials,* 2008, **7**, (1), pp: 31-37.

[35] Ansys HFSS, High Frequency Structure Simulator [Online]. Available: www. Ansys.com

[36] CST Microwave Studio, Computer Simulation Technology [Online]. Available: www.cst.com